phys. stat. sol. (b) **241**, No. 10, 2345–2352 (2004) / **DOI** 10.1002/pssb.200404890

A spectroscopic view of electron–phonon coupling at metal surfaces

S.-J. Tang[1], **Junren Shi**[2], **Biao Wu**[2,3], **P. T. Sprunger**[4], **W. L. Yang**[5,6], **V. Brouet**[5,6], **X. J. Zhou**[5], **Z. Hussain**[6], **Z.-X. Shen**[5], **Zhenyu Zhang**[1,2], and **E. W. Plummer**[*,1,2]

[1] Department of Physics and Astronomy, University of Tennessee, Knoxville, TN 37996, USA
[2] Condensed Matter Sciences Division, Oak Ridge National Laboratory, Oak Ridge, TN 37831, USA
[3] Department of Physics, University of Texas, Austin, TX 78712, USA
[4] Department of Physics and Astronomy, Louisiana State University, Baton Rouge, LA 70803, USA
[5] Department of Physics, Applied Physics and Stanford Synchrotron Radiation Laboratory, Stanford University, Stanford, CA 94305, USA
[6] Advanced Light Source, Lawrence Berkeley National Laboratory, Berkeley, CA 94720, USA

Received 9 January 2004, revised 26 May 2004, accepted 27 May 2004
Published online 13 July 2004

PACS 63.22.+m, 68.35.Ja, 73.20.–r

It is now possible to extract from high-resolution angle-resolved photoemission data the Eliashberg function $\alpha^2F(\omega)$ for electron-phonon coupling (EPC). At the same time, first-principles calculations of the EPC for surface states are appearing in the literature presenting an exquisite picture of the origin of the Eliashberg function. The advances in this field will be illustrated with new data from surface states on two faces of berylium and a direct comparisin to theory for Be(0001).

1 Introduction

Electron–phonon coupling (EPC) is the basis for many interesting phenomena in condensed matter physics [1–4]. Recent advances in experimental techniques and theoretical capabilities associated with the study of surfaces promise to reveal a spectroscopic picture of EPC. High-resolution angle-resolved photoemission is producing direct images of the distortion of the two-dimensional surface state bands near the Fermi energy caused by EPC [5–11]. First-principles calculations of the EPC for surface states are appearing in the literature [12–14] which not only explain the origin of the EPC-induced band distortions but also produce exquisite pictures of the Eliashberg function $\alpha^2F(\omega)$ [14]. The Eliashberg function is the product of a coupling constant and the phonon density of states and is at the heart of any theory of EPC [1]. A recent theoretical advance that will be described in this paper will allow experimentalists to extract the Eliashberg function directly from the high-resolution photoemission data [9]. These developments mark the beginning of a new era and a renaissance in the elucidation of many-body effects in reduced dimensionality.

In the 1960s, the most definitive signature for determining the mechanism in conventional superconductors was the measurement of the single-particle tunneling I–V characteristic [15] and the concomitant inversion procedure to display the Eliashberg function [16]. Today EPC is intimately associated with the functionality of complex materials [2] and its role in high-T_C superconductivity is being actively discussed [3, 4]. Research on metal surfaces can produce an unprecedentedly detailed picture of EPC. The Eliashberg function can be measured as a function of both E and $\boldsymbol{k}$ and related directly to measured and calculated surface phonon dispersion.

[*] Corresponding author: e-mail: eplummer@utk.edu, Phone: +001 865 974 2288, Fax: +001 865 974 3895

These investigations on surfaces of relatively simple metals can be the platform for understanding functionality in complex materials associated with the coupling between charge and lattice. In this paper, experiment and theory will be compared for EPC observed for surface states on two faces of beryllium.

2 Analysis of photoemission data

All characteristics of EPC are described by the Eliashberg function $E(\omega, \varepsilon, \boldsymbol{k}) = \alpha^2(\omega, \boldsymbol{k})F(\omega, \varepsilon, \boldsymbol{k})$, the total transition probability of a quasi-particle from/to the state $(\varepsilon, \boldsymbol{k})$ by coupling to phonon modes of frequency ω [1]. Theoretically all quantities associated with EPC can be deduced from this function, for example the mass enhancement factor λ is related to the Eliashberg function by [1]

$$\lambda = 2\int_0^\infty \frac{\mathrm{d}\omega}{\omega}\alpha^2 F(\omega)\,. \tag{1}$$

Information about the Eliashberg function can be obtained from the angle-resolved photoemission spectra, both through the EPC distortion of the quasi-particle bands near the Fermi energy and the temperature-dependent linewidth. If $\varepsilon_0(\boldsymbol{k})$ is the bare quasi-particle dispersion of a surface state without EPC, then the measured dispersion $\varepsilon(\boldsymbol{k})$ with EPC is given by

$$\varepsilon(\boldsymbol{k}) = \varepsilon_0(\boldsymbol{k}) + \mathrm{Re}\ \Sigma(\boldsymbol{k}, \varepsilon)\,. \tag{2}$$

The screening of the electrons by the lattice is represented by the self-energy function $\Sigma(\boldsymbol{k}, \varepsilon)$. The imaginary part of the self-energy is related to the EPC contribution to the lifetime τ of the excited electronic states,

$$\tau^{-1} = 2\ \mathrm{Im}\ \Sigma(\boldsymbol{k}, \varepsilon, T). \tag{3}$$

In this case, the temperature dependence of Im Σ will give the temperature-dependent linewidth. This dependency of the linewidth upon temperature has been used to extract a mass enhancement factor λ for energies ε much larger than the scale of the phonon band width [see references in 11].

In general, the electronic bandwidth is large compared with the phonon bandwidth so the ε dependence is negligible in $E(\omega, \varepsilon, \boldsymbol{k})$. For brevity, the $\boldsymbol{k}$ dependence will also be dropped. Then, $E(\omega) = \alpha^2(\omega)F(\omega)$, which is usually written as $E(\omega) = \alpha^2 F(\omega)$. With this formulation, the Re $\Sigma(\varepsilon, T)$ is

$$\mathrm{Re}\,\Sigma(\varepsilon;T) = \int_0^\infty \mathrm{d}\omega G\left(\frac{\varepsilon}{kT}, \frac{\omega}{kT}\right)E(\omega) \tag{4}$$

with the function G given by

$$G(y,z) = \int_{-\infty}^{\infty}\mathrm{d}x\frac{2z}{x^2 - z^2}f(x-y)\,. \tag{5}$$

The $\mathrm{Im}\,\Sigma(\varepsilon, T)$ is defined by the following equation:

$$\mathrm{Im}\,\Sigma(\varepsilon, T) = \pi\int_0^\infty \mathrm{d}\omega E(\omega)[1 - f(\varepsilon-\omega) + f(\varepsilon+\omega) + 2n(\omega)]\,, \tag{6}$$

where f and n are the Fermi and Bose distribution functions, respectively.

The challenge is to extract the Eliashberg function from Eqs. (5) and (6) by integral inversion [9].

3 Extraction of the Eliashberg function from data on Be(10$\bar{1}$0)

The most straightforward way to do the integral inversion is the least-squares approach. Unfortunately, because of the data noise inevitably present, such a straightforward approach fails to provide any useful

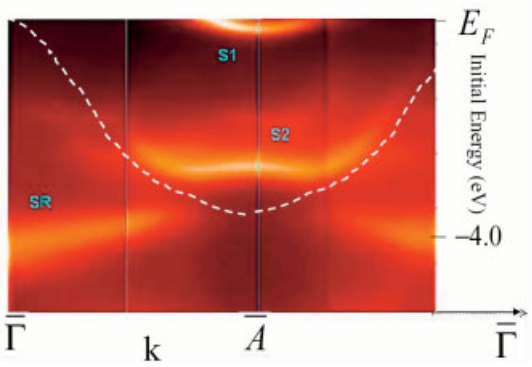

Fig. 1 (online colour at: www.pss-b.com) Energy vs. momentum photoemission display of the two surface state bands S1 and S2 on Be(10$\bar{1}$0) [9]. The dashed line is the bulk band edge. Data taken at 30 K at ALS beamline 10.0.1 at 40 eV photon energy.

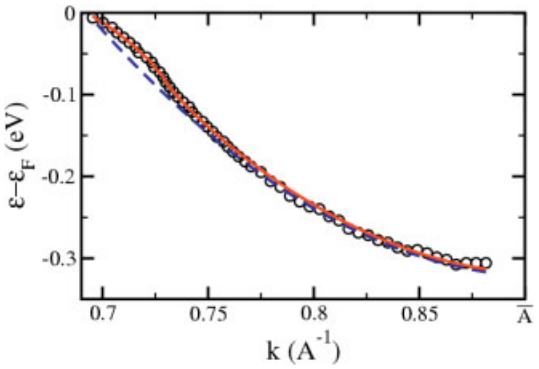

Fig. 2 (online colour at: www.pss-b.com) Quasi-particle dispersion determined from momentum distribution curves (circles) obtained at 24 eV photon energy. Dashed blue line is the bare particle dispersion $\varepsilon_0(k)$ and the red line is the fit to the data from the extracted Eliashberg function.

information because the inversion process defined by Eqs. (4)–(5) is ill-posed mathematically and the direct inversion tends to exponentially amplify the high-frequency data noise. This results in great fluctuations and negative values in the extracted Eliashberg function [18]. The failure of the least-squares method originates from the fact that no physical constraints (*priori* knowledge) are used in the fitting process. For example, one obvious constraint is that the Eliashberg function must be positive. The standard way to incorporate these constraints in the fitting process is the Maximum Entropy Method (MEM) [19–21]. The physical constraints are built into *constraint function* for the fitting procedure.

The first application of MEM to angle-resolved photoemission data was for the S1 surface state on Be(10$\bar{1}$0) [9]. The data, Re $\Sigma(\varepsilon)$, and extracted Eliashberg function are shown in Figs. 1–4. Figure 1 is the Energy vs. Momentum display of the two surface states near the Surface Brillouin Zone (SBZ) boundary $\bar{A}$ [22–24]. Figure 2 is an expanded view of the S1 surface state dispersion in the $\bar{\Gamma} \to \bar{A}$ direction of the SBZ. The blue dashed line is the bare quasi-particle dispersion $\varepsilon_0(k)$ (effective mass 0.56) and the circles are measured quasi-particle dispersion $\varepsilon(k)$. Notice the distortion near the Fermi energy caused by EPC [9]. Figure 3 displays the Re $\Sigma(\varepsilon)$ determined from the data in Fig. 2 using Eq. (2). The solid red line is the MEM fit to the data using a simple constraint function $m(\omega)$ containing the following physics. (a) The low frequency portion must look like a Debye-model (i.e., the function goes to zero at $\omega = 0$). (b) The function must be positive for all values of ω. (c) There is a highest frequency above which the Eliashberg function is zero (i.e., top of the phonon bands). A generic form of $m(\omega)$ is

$$m(\omega) = \begin{cases} m_0(\omega_R)^2, & \omega \le \omega_R \\ m_0, & \omega_R < \omega \le \omega_m. \\ 0, & \omega > \omega_m \end{cases} \tag{7}$$

The details and tests of this MEM fitting procedure are described in Ref. [9]. Figure 4 shows the extracted Eliashberg function at the Fermi surface EPC of the S1 surface state on Be(10$\bar{1}$0) (black curve). The red curve is the bulk phonon density of states [25].

When the extracted Eliashberg function is compared with experimental data [26] or first-principles calculations [27] of the surface phonon dispersion, there is an excellent correspondance [9]. The mass enhancement factor obtained from the extracted Eliashberg function using Eq. (1) is 0.68 ± 0.08 (λ_{bulk} = 0.24), consistent with $\lambda = 0.65$ obtained from measurments of the temperature dependence of the photoemission linewidth at $\bar{A}$ [24]. More than 75% of the mass enhancement λ (0.51 out of 0.68) originates from low-frequency surface modes with energy less than 45 meV. This raises a question, whether the

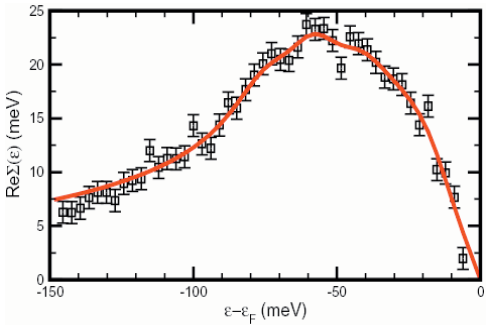

Fig. 3 (online colour at: www.pss-b.com) Re $\Sigma(\varepsilon)$ obtained from the experimental data shown in Fig. 2. The red curve is the MEM fitting of the data [9].

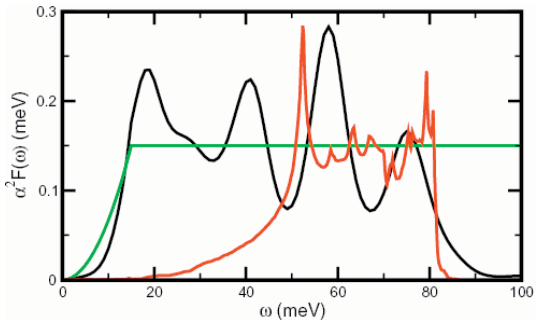

Fig. 4 (online colour at: www.pss-b.com) Black curve is the extracted Eliashberg function using the contraint function of Eq. (7) (green line) and the red curve is the bulk phonon density of states in Be [25].

low-frequency phonon modes indicative of a surface are the origin of the enhanced-EPC measured at surfaces [11]. One measure of the importance of the average phonon energy, which is usually represented by

$$\ln \omega_{\log} = \frac{2}{\lambda} \int_0^\infty \frac{\mathrm{d}\omega}{\omega} \alpha^2 F(\omega) \ln \omega \,. \tag{8}$$

When this average phonon frequency is calculated using the extracted Eliashberg function, a value of 29 meV is obtained which should be compared to ~60 meV for the bulk. The final comment is that the Re $\Sigma(\varepsilon)$ shown in Fig. 3 cannot be fitted with any simple representation of the phonon density of states, such as a Debye or Einstein model [7].

4 A comparison of experiment and theory on Be(0001)

Be(0001) has been the most studied surface with respect to enhanced EPC of surface states. There are several experiments and a first-principles calculation reported in the literature [6, 7, 9, 28] and the electronic [29–32], vibrational [28], and structural [33] properties have been reported. Figure 5 displays the properties of the surface states on the Be(0001) surface. The temperature dependence of the photoemission linewidth from the surface state at $\bar{\Gamma}$ in the SBZ was reported in 1998 [28], yielding a value of $\lambda = 1.15$. The authors speculated about superconductivity at the surface [28], but in a later paper pointed out that the original analysis was incorrect because of the curvature of the band at $\bar{\Gamma}$, and that the correct value was $\lambda = 0.87$ [7]. In 1999, the first measurement of $\lambda(E_F) = 1.18$ (12 K) was reported [6]. In 2000, a measurement of Re $\Sigma(\varepsilon)$ at 40 K gave $\lambda = 0.7 \pm 0.1$ [7].

First-principles calculations of the EPC for Be(0001) furnish a spectroscopic picture of EPC (i.e., the Eliashberg function) [14]. Figure 6 shows the calculations for the decay of a hole at the Fermi energy (a)

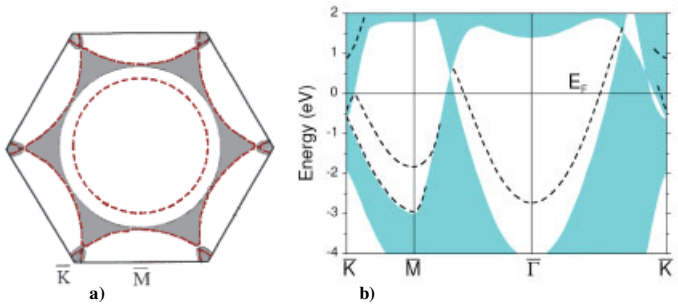

Fig. 5 (online colour at: www.pss-b.com) Electronic properties of Be(0001), shaded areas are the projection of the bulk bands onto the surface and the dashed lines are surface states: (a) The SBZ and states at E_F. (b) The two high symmetry directions showing E vs. k [29–32].

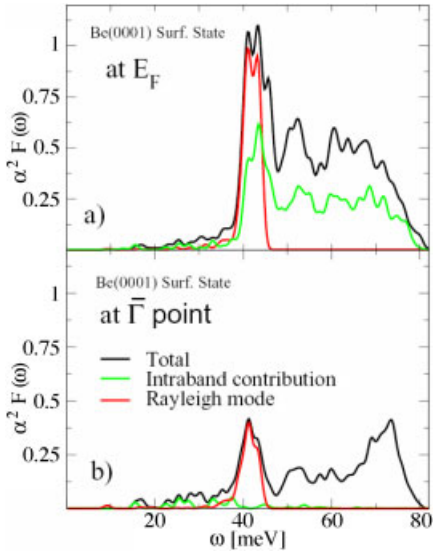

Fig. 6 (online colour at: www.pss-b.com) Calculated Eliashberg functions for the surface state on Be(0001) [14]. (a) is for a hole at E_F and (b) is for a hole at the bottom of the band. The red curve shows the different coupling to the Surface Rayleigh phonon mode.

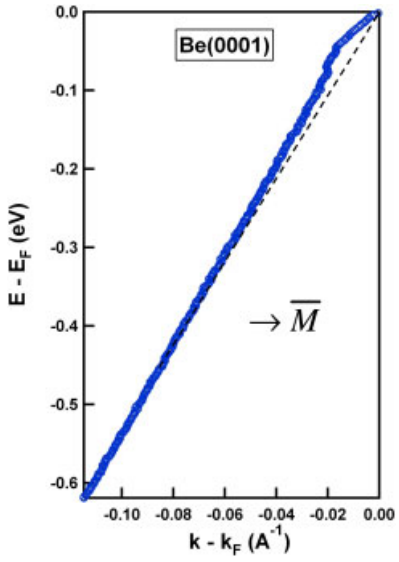

Fig. 7 (online colour at: www.pss-b.com) Quasi-particle dispersion for Be(0001) surface state determined from momentum distribution curves (blue) obtained at 40 eV photon energy. Dashed black line is the bare particle dispersion $\varepsilon_0(k)$, $k_F = 0.947$ Å^{-1}.

and at the bottom of the surface state band (b) [14]. The first message is that the Eliashberg function is very different at the Fermi energy compared to the bottom of the band. If Eq. (1) is used to calculate the mass enhancement factor, there is a dramatic energy dependence $\lambda(E_F) = 0.87$ but $\lambda(\bar{\Gamma}) = 0.37$. The fact that λ for a surface state should be a function of ε was pointed out in 1996 [34]. The second message is that the scattering or decay mechanism of a hole at E_F and at the bottom of the surface state band is quite different. The decay of a hole at the Fermi energy is dominated by the intraband scattering contribution (green line) and by the Rayleigh mode scattering (red line). If decay into the surface state at the $\bar{M}$ point in the SBZ (Fig. 5) is included, then 90% of the total (black) is from surface process. In contrast, the bulk interband decay modes dominate at $\bar{\Gamma}$.

The question to be addressed in this section is, Why are the experimental results at variance with the theory and with each other? One possibility is that there is strong $\boldsymbol{k}$ dependence in the Eliashberg function [i.e., $E(\boldsymbol{k}, \omega)$]. Theory was for the $\bar{\Gamma} \rightarrow \bar{K}$ direction, while the experiments were in the $\bar{\Gamma} \rightarrow \bar{M}$ direction [6] and half way between these two directions [7] (see Fig. 5). A second and more plausible explanation is that the data is not good enough. A third explanation is that there are deficiencies in the theory. We will compare the existing data and calculations with new data taken at the Advanced Light Source (ALS).

The Be(0001) surface state band dispersion in the $\bar{\Gamma} \rightarrow \bar{M}$ direction (Fig. 5) was measured at ALS on beamline 10.0.1. The sample cleaning has been described previously. The measurements reported here were made at 40 eV photon energy, with a total resolution of ~15 meV. The sample temperature was 25 K. The quasi-particle dispersion was determined using momentum distribution curves and is shown in Fig. 7. The bare particle dispersion was determined using a linear equation for the dispersion near the Fermi energy, with $k_F(M) = 0.947$ Å^{-1}. Re $\Sigma(\varepsilon)$ determined from the data in Fig. 7 is shown in Fig. 8 and compared with the data reported earlier by LaShell et al. [7]. It is obvious that there is structure in the Re Σ at energies of ~25, 45, and 65 meV. The MEM method was used to fit the Re $\Sigma(\varepsilon)$ for both the new data and the previously published data of LaShell et al. [7]. The fit to both sets of data is shown in Fig. 8. It is obvious that the two data sets are very different and consequently the extracted Eliashberg functions will be quite different. The red curve is calculated using the theoretical Eliashberg function from Ref. [14].

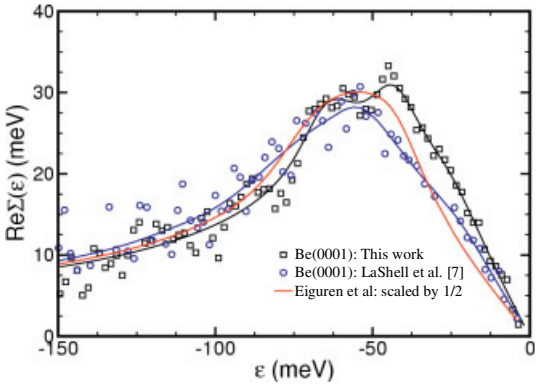

Fig. 8 (online colour at: www.pss-b.com) Fit to the Re $\Sigma(\varepsilon)$ from data [7]. The red line is the Re $\Sigma(\varepsilon)$ calculated from the theoretically derived $\alpha^2F(\omega)$ [14].

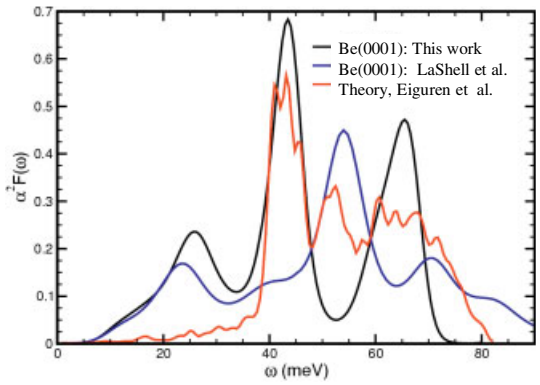

Fig. 9 (online colour at: www.pss-b.com) Elisahberg functions, black from this work, blue from the data in LaShell et al. [7], and red from the theoretical calculation by Eiguen et al. [14].

To get this theoretical curve to agree with the data, it had be be scaled by 1/2. In all cases, the Re $\Sigma(\varepsilon)$ has been calculated for the temperature of the experiment, 40 K for the LaShell et al., data [7] and 25 K for the new data.

The extracted Eliashberg functions are shown in Fig. 9 and compared to the theoretical curve [12]. It is obvious that all three are different. The question is why? The three possiblities were outlined earlier. The most interesting physical explanation is that there is a strong ***k*** dependence in the Eliashberg function, even for Be(0001). All three of the Eliashberg functions are for a different point on the surface state Fermi contour (Fig. 5). Another obvious difference between both experimental derived curves and the theoretical curve is the weight in the low energy part of the spectrum in the experimental curves. One way to quantify this difference is to use Eq. (8) to calculate the average $\omega_{\log}$ (see Table 1). A possible reason for the difference between theory and experiment in the low-frequency region is that the 12-layer slab calculation used to calculate the phonon dispersion [14] does not accurately reproduce anomalies in the experimental data [25]. Mesurements of the surface phonon dispersion on Be(0001) showed that for small q the Rayleigh mode had a slope 30% larger than the bulk sound wave velocity and consequently was inside the bulk phonon continuum as shown in Fig. 10 [25]. The Rayleigh mode emerges from the continuum at approximately the energy where the structure is seen in the experimental Eliashberg function (~25 meV). Table 1 summarizes all of the measured and extracted EPC parameters for the surface state on Be(0001).

Table 1 Comparison of the measured and calculated mass enhancement factors λ for the surface state on Be(0001).

λ	$\omega_{\log}$(meV)	k is SBZ	T	procedure	reference
0.87		$\bar{\Gamma}$	variable	Im $\Sigma(T)$	[7, 28]
1.18		$\bar{\mathrm{M}}$	12 K	d Re $\Sigma(\varepsilon)$/dε	[6]
0.7 ± 0.1		$\bar{\mathrm{M}} \leftrightarrow \bar{\mathrm{K}}$	40 K	Fitting Re $\Sigma(\varepsilon)$ with Debye model	[7]
0.37		$\bar{\Gamma}$	0 K	First principles calculations	[14]
0.87		$\bar{\mathrm{K}}$	0 K	First principles calculation	[14]
0.70 ± 0.08	33.6	$\bar{\mathrm{M}}$	0 K	MEM extracted $\alpha^2F(\omega)$	this work
0.59 ± 0.07	35.7	$\bar{\mathrm{M}} \leftrightarrow \bar{\mathrm{K}}$	0 K	MEM extracted $\alpha^2F(\omega)$ from [7]	this work
0.88	49.0	$\bar{\mathrm{K}}$	0 K	Calculated from $\alpha^2F(\omega)$ of [14]	this work

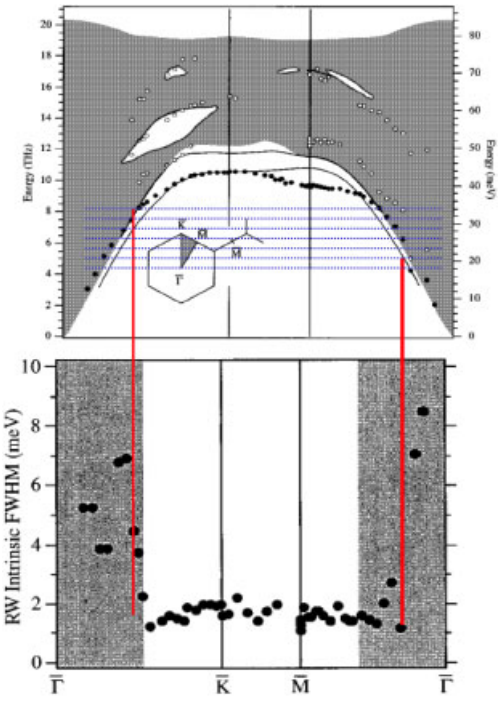

Fig. 10 (online colour at: www.pss-b.com) Linewidth changes in the Rayleigh mode on Be(0001) [25]. Blue horizontal lines indicate the ω region of the low-frequency peaks in Fig. 9.

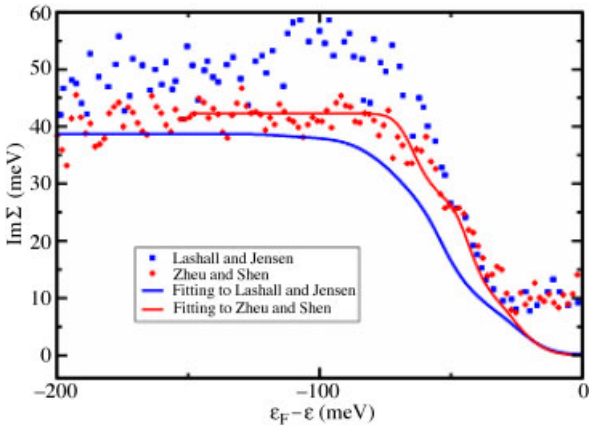

Fig. 11 (online colour at: www.pss-b.com) Im $\Sigma(\varepsilon)$ for the surface state on Be(0001). The solid red (blue) curve is calculated using Eq. (6) and the black (blue) extracted Eliashberg function shown in Fig. 9. The red dots (Zhou and Shen) are from the data presented here and the blue dots from LaShell et al. [7].

Im $\Sigma(\varepsilon)$ can be calculated using the extracted Eliashberg function (Eq. (6)) and compared to the experimentally determined Im $\Sigma(\varepsilon)$. This procedure offers an easy self-consistency check for the extraction procedure. Experimentally, $\mathrm{Im}\,\Sigma(\varepsilon) = \hbar\Gamma v_0/2$ with Γ being the FWHM determined from the momentum distribution curves and v_0 is the bare particle velocity. Figure 11 displays Im $\Sigma(\varepsilon)$, both determined experimentally (blue and red dots) and calculated from the extracted Eliashberg functions shown in Fig. 9. The solid red curve is Im $\Sigma(\varepsilon)$ calculated using the Eliashberg function extracted from our data (black curve in Fig. 8). There is quite remarkable agreement with the experimentally determined curve (red dots). In contrast, the Im $\Sigma(\varepsilon)$ calculated from the Eliashberg function extracted from the LaShell et al. data [7] (blue curve in Fig. 9) does not agree with the measured curve (blue dots). This discrepancy is undoubtedly due to the procedure used to determine the bare particle dispersion in the work of LaShell et al. [7]. It is also possible to determine Re $\Sigma(\varepsilon)$ from Im $\Sigma(\varepsilon)$ using a Hilbert transform [35], but the result will be quite sensitive to the choice of the bare particle dispersion.

5 Conclusion

Recent developments hold significant promise for having surface states on metal surfaces become the playground for EPC physics. Text book examples elucidating the origin and nature of EPC in reduced dimensionality will come. At the same time the understanding developed with these prototype systems can lead to a better understanding of EPC in complex systems.

Acknowledgements This work was supported by NSF (EWP) DMR 0105232. The experiment was performed at the ALS of LBNL, which is operated by the DOE's Office of BES, Division of Materials Science and Engineering,

under contract DE-AC03-76SF0098. The work at Stanford was supported by NSF grant DMR-0071897. The theory was supported by Oak Ridge National Laboratory, managed by UT-Battelle, LLC, for the U.S. Department of Energy under Contract DE-AC05-00OR22725.

References

[1] G. Grimvall, The Electron-Phonon Interaction in Metals, Selected Topics in Solid State Physics, edited by E. Wohlfarth (North-Holland, New York, 1981).
[2] D. M. Edwards, ArXiv:cond-mat/0201558 (2002).
[3] T. Egami, J. Supercond. **15**, 373 (2002);
T. Egami and P. Piekarz, Solid State Commun. (to be published).
[4] A. Damascelli, Z. Hussain, and Z.-X. Shen, Rev. Mod. Phys. **75**, 473 (2003).
[5] T. Valla, A. V. Fedorov, P. D. Johnson, and S. L. Hulbert, Phys. Rev. Lett. **83**, 2085 (1999).
[6] M. Hengsberger, D. Purdie, P. Segovia, M. Garnier, and Y. Baer, Phys. Rev. Lett. **83**, 592 (1999).
M. Hensberger, R. Frésard, D. Purdie, P. Segovia, and Y. Baer, Phys. Rev. B **60**, 10796 (1999).
[7] S. LaShell, E. Jensen, and T. Balasubramanian, Phys. Rev. B **61**, 2371 (2000).
[8] E. Rotenberg, J. Schaefer, and S. D. Kevan, Phys. Rev. Lett. **84**, 2925 (2000).
[9] J. Shi, S.-J. Tang, Biao Wu, P. T. Sprunger, W. L. Yang, V. Brouet, X. J. Zhou, Z. Hussain, Z.-X. Shen, Z. Zhang, and E. W. Plummer, Phys. Rev. Lett. **92**, 186401 (2004).
[10] S. D. Kevan and Eli Rotenberg, J. Electron Spectrosc. **117–118**, 57 (2001).
[11] E. W. Plummer, J. Shi, S.-J. Tang, E. Rotenberg, and S. D. Kevan, Prog. Surf. Sci. **74**, 251 (2003).
[12] A. Eiguren, B. Hellsing, F. Reinert, G. Nicolay, E. V. Chulkov, V. M. Sinkin, S. Hüfner, and P. M. Echenique, Phys. Rev. Lett. **88**, 066805 (2002).
[13] A. Eiguren, B. Hellsing, E. V. Chulkov, and P. M. Echenique, Phys. Rev. B **67**, 235423 (2003).
[14] A. Eiguren, S. de Gironcoli, E. V. Chulkov, P. M. Echenique, and E. Tosatti, Phys. Rev. Lett. **91**, 166803 (2003).
[15] J. M. Rowell, P. W. Anderson, and D. E. Thomas, Phys. Rev. Lett. **10**, 334 (1963).
[16] W. L. McMillan and J. M. Rowell, Phys. Rev. Lett. **14**, 108 (1965).
Q. Wang, Y. Yang, and R. Wang, phys. stat. sol. (a) **155**, 289 (1996).
[17] S. Verga, A. Knigavko, and F. Marsiglio, Phys. Rev. B **67**, 054503 (2003).
[18] J. Skilling, Maximum Entropy and Bayesian Methods (Kluwer Academic, Dordrecht, 1989).
[19] J. E. Gubernatis, M. Jarrell, R. N. Silver, and D. S. Sivia, Phys. Rev. B **44**, 6011 (1991).
[20] R. K. Bryan, Eur. Biophys. J. **18**, 165 (1990).
[21] V. M. Silkin and E. W. Chulkov, Phys. Solid State **37**, 1540 (1995).
[22] Ph. Hofmann, R. Stumpf, V. M. Silkin, E. V. Chulkov, and E. W. Plummer, Surf. Sci. Lett. **355**, L278 (1996).
[23] S.-J. Tang, Ismail, P. T. Sprunger, and E. W. Plummer, Phys. Rev. B **65**, 235428 (2002).
[24] J. B. Hannon, E. J. Mele, and E. W. Plummer, Phys. Rev. B **53**, 2090 (1996).
[25] Ph. Hofmann and E. W. Plummer, Surf. Sci. **377–379**, 330 (1997).
[26] M. Lazzeri and S. de Gironcoli, Surf. Sci. **454–456**, 442 (2000).
[27] T. Balasubramanian, E. Jensen, X. L. Wu, and S. L. Hulbert, Phys. Rev. B **57**, R6866 (1998).
[28] E. V. Chulkov, V. M. Silkin, and E. N. Shirykalov, Surf. Sci. **188**, 287 (1987).
[29] U. O. Karlsson, S. A. Flodstrom, R. Engelhardt, W. Gadeke, and E. E. Koch, Solid State Commun. **49**, 711 (1984).
[30] R. Bartynski, E. Jensen, T. Gustafsson, and E. W. Plummer, Phys. Rev. B **32**, 1921 (1985).
[31] R. Stumpf, J. B. Hannon, P. J. Feibelman, and E. W. Plummer, Electronic Surface and Interface States on Metallic Systems, edited by E. Bertel and M. Donath (World Scientific, Singapore, 1995), p. 151.
[32] H. L. Davis, J. B. Hannon, K. B. Ray, and E. W. Plummer, Phys. Rev. Lett. **68**, 2632 (1992).
[33] R. Matzdorf, G. Meister, and A. Goldmann, Phys. Rev. B **54**, 14807 (1996).
[34] C. R. Ast and H. Höchst, Phys. Rev. B **66**, 125103 (2002).